



Bioinspired engineering ADSC nanovesicles thermosensitive hydrogel enhance autophagy of dermal papilla cells for androgenetic alopecia treatment

Jiachao Xiong^{a,b,1}, Zhixiao Liu^{c,1}, Lingling Jia^{a,1}, Yulin Sun^{a,b,1}, Rong Guo^a, Tingting Xi^a, Zihan Li^d, Minjuan Wu^{c,***}, Hua Jiang^{a,**}, Yufei Li^{a,*}

^a Department of Plastic Surgery, Shanghai East Hospital, School of Medicine, Tongji University, Shanghai, 200120, China

^b Medical College, Tongji University, Shanghai, 200331, China

^c Department of Histology and Embryology, Naval Medical University, Shanghai, 200433, China

^d St Hugh's College, University of Oxford, OX2 6LE, United Kingdom

ARTICLE INFO

Keywords:

Androgenic alopecia
Nanovesicles
JAM-A
Autophagy
Hydrogel

ABSTRACT

Androgenic alopecia (AGA) is a highly prevalent form of non-scarring alopecia but lacks effective treatments. Stem cell exosomes have similar repair effects to stem cells, suffer from the drawbacks of high cost and low yield yet. Cell-derived nanovesicles acquired through mechanical extrusion exhibit favorable biomimetic properties similar to exosomes, enabling them to efficiently encapsulate substantial quantities of therapeutic proteins. In this study, we observed that JAM-A, an adhesion protein, resulted in a significantly increased the adhesion and resilience of dermal papilla cells to form snap structures against damage caused by dihydrotestosterone and macrophages, thereby facilitating the process of hair regrowth in cases of AGA. Consequently, adipose-derived stem cells were modified to overexpress JAM-A to produce engineered JAM-A overexpressing nanovesicles (JAM-A^{OE}@NV). The incorporation of JAM-A^{OE}@NV into a thermosensitive hydrogel matrix (JAM-A^{OE}@NV Gel) to effectively addresses the limitations associated with the short half-life of JAM-A^{OE}@NV, and resulted in the achievement of a sustained-release profile for JAM-A^{OE}@NV. The physicochemical characteristics of the JAM-A^{OE}@NV Gel were analyzed and assessed for its efficacy in promoting hair regrowth in vivo and vitro. The JAM-A^{OE}@NV Gel, thus, presents a novel therapeutic approach and theoretical framework for promoting the treatment of low cell adhesion diseases similar to AGA.

1. Introduction

Androgenic alopecia (AGA) is a highly prevalent form of non-scarring alopecia that affects both genders, with a prevalence reaching up to 80% in males and 50% in females [1]. Despite its high prevalence, AGA still lacks effective treatments. Currently, the most commonly utilized treatments for AGA include pharmacologic and surgical interventions [2,3]. However, its extensive clinical application of both intervention is frequently constrained by several adverse effects [4–6]. As a result, there is an urgent need for the development of effective and

risk-free therapies for AGA to compensate for the inadequacy of existing therapies.

Stem cell-derived exosomes are widely utilized in tissue repair due to possess the ability to transport various biological components, including proteins, lipids, and non-coding RNAs, which can regulate the biological activity of target cells via membrane fusion or endocytosis [7]. However, the exorbitant expense and negligible yield associated with exosome isolation represent a significant obstacle that exosome therapies must surmount immediately [8]. Cell-derived nanovesicles (CNVs) are acquired through the mechanical extrusion process of donor cells [9].

Peer review under responsibility of KeAi Communications Co., Ltd.

* Corresponding author.

** Corresponding author.

*** Corresponding author.

E-mail addresses: minjuanwu@163.com (M. Wu), dosjh@126.com (H. Jiang), lufylee@hotmail.com (Y. Li).

¹ These authors contributed equally.

<https://doi.org/10.1016/j.bioactmat.2024.02.023>

Received 23 November 2023; Received in revised form 27 January 2024; Accepted 19 February 2024

2452-199X/© 2024 The Authors. Publishing services by Elsevier B.V. on behalf of KeAi Communications Co. Ltd. This is an open access article under the CC BY-NC-ND license (<http://creativecommons.org/licenses/by-nc-nd/4.0/>).

These CNVs exhibit biomimetic properties similar to exosomes, making them a promising solution to overcome the technical challenges associated with exosome therapy [9]. Moreover, CNVs can be produced at a significantly reduced cost compared to exosomes, amounting to only 10% of the expense. However, in terms of quantity, CNVs have the potential to generate up to 100 times more material than exosomes. In light of these attributes, we have introduced and investigated the potential of adipose-derived stem cells nanovesicles (ADSC-NVs) in enhancing the efficacy of hair regrowth in AGA.

Indeed, a crucial foundation for attaining effective damage repair is the remarkable capability of CNVs to serve as vehicles for the delivery of drugs, genes, and proteins. In this content, emerging studies demonstrated that engineering methods have been used to transform CNVs, achieving precise treatment of diseases [10]. For instance, Tao et al. [11] prepared CNVs with high content of lncRNA-H19, which significantly accelerating the healing of diabetic wounds by promoting vascular regeneration. Liu et al. [12] constructed engineered CNVs that can smoothly cross the blood-brain barrier and achieve targeted therapy for tumors. Therefore, engineered CNVs could likewise be a potential novel therapeutic approach to achieve efficient hair regeneration in AGA.

In this study, we found that ADSC-NVs has a superior hair regrowth promoting effect than nanoparticles derived from human skin fibroblasts (HSF-NVs). Junctional adhesion molecule A (JAM-A) protein plays a crucial role in ADSC-NVs-mediated AGA hair regrowth, JAM-A protein transferred by ADSC-NVs promotes autophagy of dermal papilla cells (DPCs), thereby enhancing the resistance of DPCs to dihydrotestosterone (DHT) and inflammatory damage. Subsequently, bio-inspired engineered ADSC-NVs with overexpressed JAM-A (JAM-A^{OE}@NV) were incorporated into poloxamer 407 hydrogel solution (JAM-A^{OE}@NV Gel) to prepare a thermosensitive sustained-release platform to achieve efficient delivery of high-yield restorative JAM-A proteins. This study proposes a novel approach to cell-free therapy for AGA with a focus on a new mechanism of ADSC-NVs-conveyed JAM-A-induced autophagy in DPCs to promote AGA hair regrowth. These findings also highlight that JAM-A^{OE}@NV Gel achieve sustained-release deliver more JAM-A proteins, providing an advanced strategy for the hair regeneration of AGA.

2. Results

2.1. Construction and characterization of CNVs

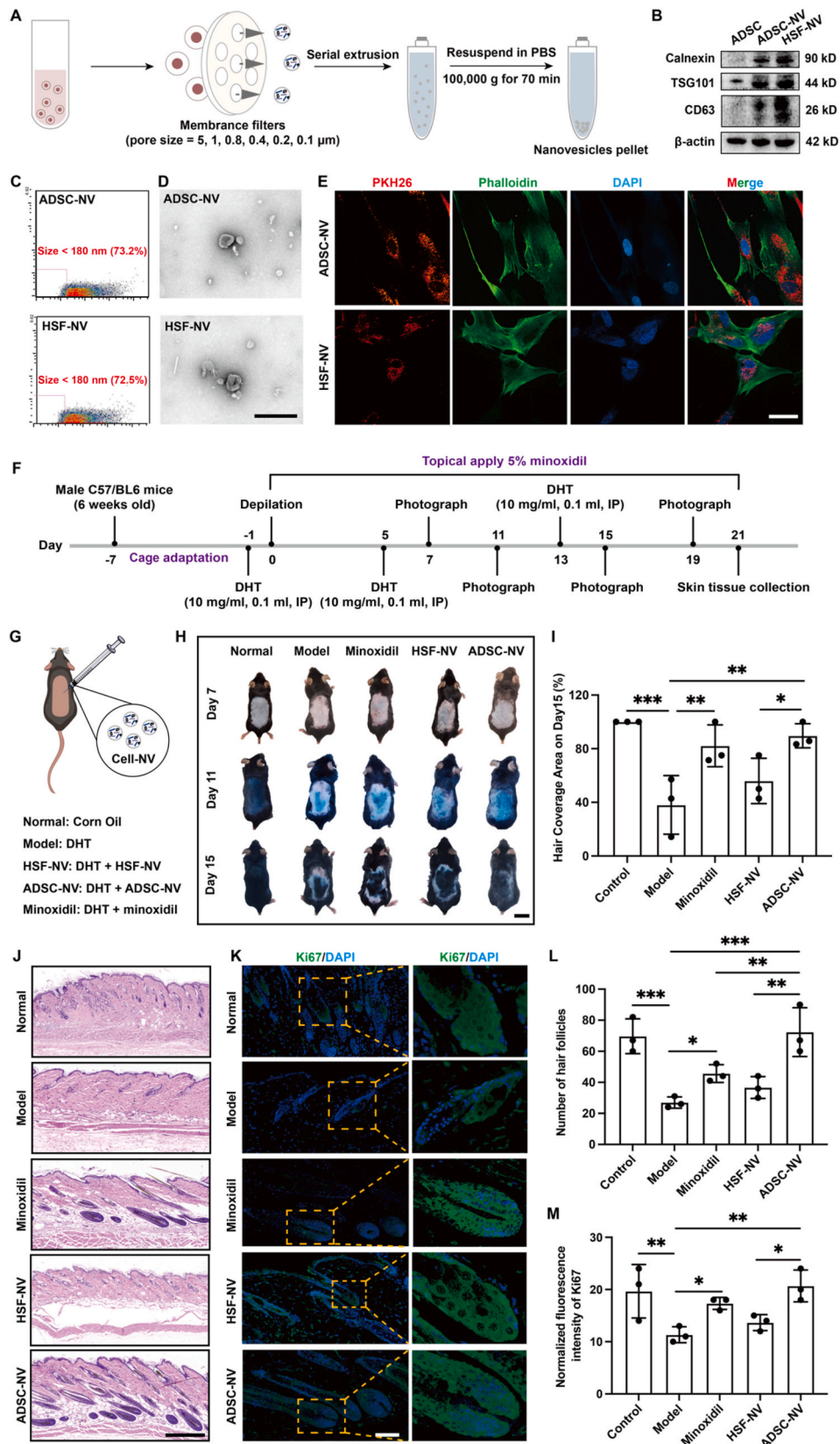
Previous studies have reported that CNVs exhibit a comparable morphology to exosomes and contain over 70% of the identical membrane proteins [13,14]. In the present study, purified CNVs were obtained using gradient-over-membrane mechanical extrusion and ultracentrifugation (Fig. 1A, Fig. S1A, Supporting Information). Subsequently, Western blotting was performed using exosome-specific protein markers (Calnexin, TSG101, and CD63) to identify CNV membrane proteins [15,16]. The findings indicated that the exosome-specific proteins were positively expressed by ADSC-NVs and HSF-NVs (Fig. 1B). The size and morphological properties of CNVs were subsequently determined using a transmission electron microscope and a NanoFlow cytometer, respectively. As evident from the findings, the majority of ADSC-NVs and HSF-NVs were found to be composed of particles smaller than 110 nm, with particles below 180 nm comprising 73.2% and 72.5% of the total fraction, respectively (Fig. 1C, Figs. S1B and C, Supporting Information). In addition, the structure of CNVs was comparable to that of exosomes, with a round cup-shaped morphology bordered by lipid membranes (Fig. 1D). On the basis of these outcomes, the purified CNVs were gathered successfully. Furthermore, PKH26-labeled CNVs exhibiting red fluorescence were co-incubated with DPCs. Subsequently, phalloidin was utilized to stain the cytoskeleton of DPCs with green fluorescence (Fig. 1E). This finding suggests that DPCs have the capability to internalize ADSC-NVs and HSF-NVs.

2.2. Effect of ADSC-NVs on hair regeneration in an AGA mice model

An average hair cycle comprises the anagen, catagen, and telogen phases. In individuals diagnosed with AGA, there is a corresponding increase in the transition of hair follicles from catagen/telogen to anagen as the anagen phase of the damaged hair follicles (HFs) becomes progressively shorter [17]. In this context, DHT comprises the key androgen implicated in the progression of AGA [18]. In order to simulate the conditions of AGA hair growth, an AGA mouse model was generated via intraperitoneal DHT injection (Fig. 1F). As a positive control, minoxidil was topically applied to the area devoid of hair. CNVs, on the other hand, were injected locally subcutaneously in multiple locations within the area affected by hair depilation, as illustrated in Fig. 1G. DHT induced a retardation of hair growth in gross examination results after hair depilation; however, this deceleration was mitigated by minoxidil and CNVs (Fig. 1H, Figs. S2A and 2C, Supporting Information). Notably, on day 15 following treatment, the ADSC-NVs group exhibited a more rapid hair growth rate in comparison to the HSF-NVs group (Fig. 1I). The skin tissue samples were collected on the 21st day after treatment, and samples were stained with hematoxylin and eosin (H&E) (Fig. 1J, Fig. S2B, Supporting Information). A near-telogen concentration of HFs was observed in the model group as a result of the effects of DHT. In contrast, the application of ADSC-NVs induced a reversible impact on DHT, resulting in a substantial augmentation in both the quantity and base enlargement of HFs (Fig. 1L, Fig. S2D, Supporting Information). Furthermore, the tissue slides were stained for Ki67 immunofluorescence and the signal strength in the HF region was assessed (Fig. 1K and M). DHT significantly decreased the number of Ki67-positive cells in the HFs, whereas treatment with ADSC-NVs increased the expression of Ki67-positive signals. These findings, therefore, indicate that ADSC-NVs have the capability to effectively reverse the delay in the HF growth cycle induced by DHT.

2.3. Protective effect of ADSC-NVs on DPCs injured by DHT and macrophages

To investigate the fundamental processes involved in the initiation and advancement of AGA, weighted gene co-expression network analysis (WGCNA) was applied to two AGA-related datasets (GSE212301 and GSE90594) obtained from the gene expression omnibus (GEO) database. The objective was to identify pertinent modular genes that exhibited a strong correlation with AGA. The optimal “soft” threshold for both datasets was determined to be $\beta = 16$ (scale-free $R^2 = 0.8$ for GSE212301, scale-free $R^2 = 0.81$ for GSE90594), and the clustered dendrograms of the normal control and AGA were presented (Figs. S3A–D, Supporting Information). The MEbrown and MEblue modules exhibited a statistically significant positive correlation with AGA, whereas the MEred and MEturquoise modules demonstrated a statistically significant negative correlation (Figs. S3E and F, Supporting Information). A Venn diagram was utilized to identify a set of sixteen negatively correlated module genes and fourteen positively correlated module genes that are shared among all modules (Figs. S4A–D, Supporting Information). Following this, co-expression network was constructed for these genes, which was subsequently utilized for enrichment analysis, including the Gene ontology (GO) and the Kyoto Encyclopedia of Genes and Genomes (KEGG) pathway (Figs. S4E–J, Supporting Information). Notably, the results of the enrichment analysis strongly indicate that the immune response and Wnt signal pathway play a crucial role in the pathogenesis of AGA. Previous studies have effectively demonstrated that scalp samples obtained from individuals diagnosed with AGA contain an assortment of inflammatory cells, including mast cells, lymphocytes, and monocytes [19,20]. These cells release significant amounts of inflammatory cytokines, leading to disruption of the HF microenvironment, which in turn manifests as a stagnation of the hair growth cycle. Furthermore, hair growth is regulated by a significant signaling pathway known as the Wnt/ β -catenin pathway [21,22]. In this



(caption on next page)

Fig. 1. Characterization of CNVs and effect of CNVs on hair regeneration in an AGA mouse model. A) Schematic of the preparation of the CNVs. B) Western blotting of exosome markers Calnexin, TSG101, and CD63. C) NanoFlow analysis of CNVs. D) Morphology of CNVs under transmission electron microscopy (TEM); scale bar: 400 nm. E) Fluorescent images of PKH26-labeled CNVs internalized by DPCs stained with phalloidin; scale bar: 40 μ m. F) Animal experimental schedule for inducing the AGA mouse model. G) Schematic diagram of animal groupings and interventions. H) Representative optical images of hair growth on days 7, 11, 15 after treatment; scale bar: 2 cm. I) The hair-covered area of the dorsal skin of mice on day 15 after treatment with different formulations. J) Representative H&E staining images of hair follicle regeneration on the dorsal skin of mice on day 21; scale bar: 400 μ m. K) Representative Ki67 immunofluorescence staining images of hair follicle regeneration on day 21; scale bar: 100 μ m. L) Statistical data on hair follicle number was counted in the same random area. M) Statistical data on the relative Ki67 expression of the different groups. (n = 3 per group, *p < 0.05, **p < 0.01, ***p < 0.001).

context, DPCs are accountable for signal reception and transmission, induction of proliferation and differentiation of HF stem cells via the Wnt/ β -catenin pathway, regulation of hair bulb size, anagen phase duration, and hair shaft diameter, and are regarded as the control centers of HF growth.

Based on the potential pathogenesis mechanisms of AGA, the DPCs models of DHT-injured and inflammation-injured were established to explore the protective effects of ADSC-NVs. The optimal concentrations of ADSC-NVs and DHT for subsequent experiments were determined by analyzing the effects of ADSC-NVs and DHT on DPC proliferation using the Cell Counting Kit-8 (CCK-8) assay (Fig. 2A, Fig. S5A, Supporting Information). ADSC-NVs had a more pronounced and enduring promotional effect on DPCs than HSF-NVs at equivalent concentrations, as shown by the CCK8 result of ADSC-NVs (Fig. S5B, Supporting Information). The most pronounced and enduring promotional effect was observed at 100 μ g/mL ADSC-NVs. In accordance with the findings of prior research indicating that DPC senescence was significantly induced by 10 nM/mL DHT, the CCK8 assay demonstrated that both 5 nM/mL and 10 nM/mL DHT had a substantial inhibitory impact on DPC proliferation [23]. As a result, a DHT concentration of 10 nM/mL was selected for the further experimental procedures.

To assess the impact of CNVs on DHT-injured DPCs proliferation, migration, and senescence, respectively, scratch assays, CCK8 proliferation assays, and the senescence-associated β -galactosidase (SA- β -gal) activity assay were employed. Both CNVs significantly promoted the proliferation of DHT-damaged DPCs, as shown in Fig. 2B; however, ADSC-NVs promoted the proliferation of DPCs more efficiently than HSF-NVs. ADSC-NVs exhibited greater efficacy in inhibiting the senescence of DPCs induced by DHT compared to HSF-NVs (Fig. 2C, Fig. S5C, Supporting Information). Moreover, an analysis of the migration performances of DPCs treated with ADSC-NVs unveiled that ADSC-NVs exhibited the most pronounced activity in promoting migration at 24 h, surpassing that of HSF-NVs at 48 h and 72 h (Figs. 2D and E). These findings indicate that ADSC-NVs are capable of effectively reversing DPCs damage induced by DHT.

The presence of tissue inflammation in the hairless region surrounding the HFs in multiple scalp biopsy studies of patients with AGA suggests that inflammation of the HFs plays a significant role in the pathogenesis of the disease [24,25]. Furthermore, an investigation was conducted using the single sample Gene Set Enrichment Analysis (ssGSEA) algorithm to examine the abundances of macrophage cytokine production, macrophage activation, and macrophage chemotaxis in the frontal alopecia region of AGA patients in GSE212301. The findings revealed significant levels of inflammatory factor production, macrophage activation, and macrophage chemotaxis within the frontal alopecia region (Fig. 2F), indicating that macrophage damage to HFs plays a significant role in the development of AGA. In order to establish a model of macrophage injury, Raw 264.7 cells were co-cultured with DPCs after being treated with lipopolysaccharide (LPS) (Fig. 2G). Subsequently, the protective effect of CNVs on a macrophage injury model was examined using an apoptosis kit (Fig. 2H). Both ADSC-NVs and CNVs exhibited a comparable pattern, with ADSC-NVs significantly reversing the apoptosis of DPCs, while HSF-NVs demonstrated less pronounced repair activity (Fig. 2I). ADSC-NVs are clearly an effective treatment for AGA hair regrowth.

2.4. JAM-A protein plays a core link in ADSC-NVs-mediated AGA hair regrowth

Cellular autophagy is a physiological process whereby cells engage in self-phagocytosis of intrinsically damaged organelles to preserve cellular equilibrium and withstand external harm [26,27]. Autophagy dysfunction is a common complication of aging, and ADSC exosomes can stimulate autophagy in order to substantially accelerate the repair of diverse tissue injuries [28–30]. In this context, Tang et al. [31] discovered that ADSC exosomes have the ability to stimulate AGA HF regeneration via the Wnt/ β -catenin pathway. Thus, the question of whether ADSC-NVs can similarly stimulate the Wnt/ β -catenin pathway and promote autophagy in DPCs damaged by DHT piqued our keen interest.

In order to ascertain autophagic activity, we discovered that ADSC-NVs promoted a greater number of autophagosomes to form in DHT-damaged DPCs, as observed by TEM (Fig. 2J). Furthermore, the protein levels of LC3 and β -catenin were assessed to evaluate the activation levels of autophagy and Wnt/ β -catenin pathways (Fig. 2K–M). The results showed that LC-3II and β -catenin expression was significantly reduced in DHT-injured DPCs, whereas ADSC-NVs significantly eliminated the inhibitory effect of DHT. These results suggest that ADSC-NVs functioned similarly to ADSC exosomes to activate autophagy and Wnt/ β -catenin pathways to promote AGA hair regeneration. However, the precise mechanism through which ADSC-NVs stimulate the expression of both pathways prompts additional investigation.

As a vital member of the JAM family, JAM-A (also referred to as F11R) is involved in cellular migration, proliferation, and permeability. Our previous study demonstrated that JAM-A could preserve the function of DPCs and stimulate HF regeneration in alopecia areata [32]. Consistent with the results of this investigation, we observed a noteworthy reduction in the expression of JAM-A in the DHT-injured DPC dataset (GSE184501) (Fig. 3A). Furthermore, we validated that ADSC-NVs could effectively counteract the DHT-induced downregulation of JAM-A protein (Fig. 2B and C). In addition, we discovered that adipose-derived stem cells (ADSCs) contain a greater quantity of JAM-A proteins than HSF, and that ADSC-NVs acquired via extrusion were capable of encapsulating and delivering a greater quantity of JAM-A proteins to mitigate DHT damage (Figs. S6A and B, Supporting Information).

In order to investigate the pivotal role played by JAM-A in damaged DPCs and the subsequent effects on the autophagy and Wnt/ β -catenin pathways, we established DPCs cell lines with JAM-A overexpression (JAM-A^{OE}), JAM-A interference (JAM-A^{Si}), and JAM-A control (JAM-A^{NC}) by lentiviral transfection (Figs. S7A and B, Supporting Information). Similarly, the cell lines were subjected to DHT and macrophage injury modeling and assayed for proliferation, migration, senescence and apoptosis indicators (Fig. 3D–I, Fig. S7C, Supporting Information). The results indicated that the downregulation of JAM-A significantly impaired the ability of DPCs to resist damage from DHT and macrophages, as demonstrated by an increase in senescent and apoptotic cells and a reduction in proliferative and migratory capacities. On the contrary, overexpression of JAM-A enabled the activation of DPCs that were effective against DHT and macrophage-induced injury.

Previous studies have reported that inhibiting JAM-A leads to the initiation of the AKT pathway [33]. While the AKT pathway has been identified as a driver of tumor cell proliferation, its activation in healthy cells can impede autophagy and accelerate cellular senescence [34].

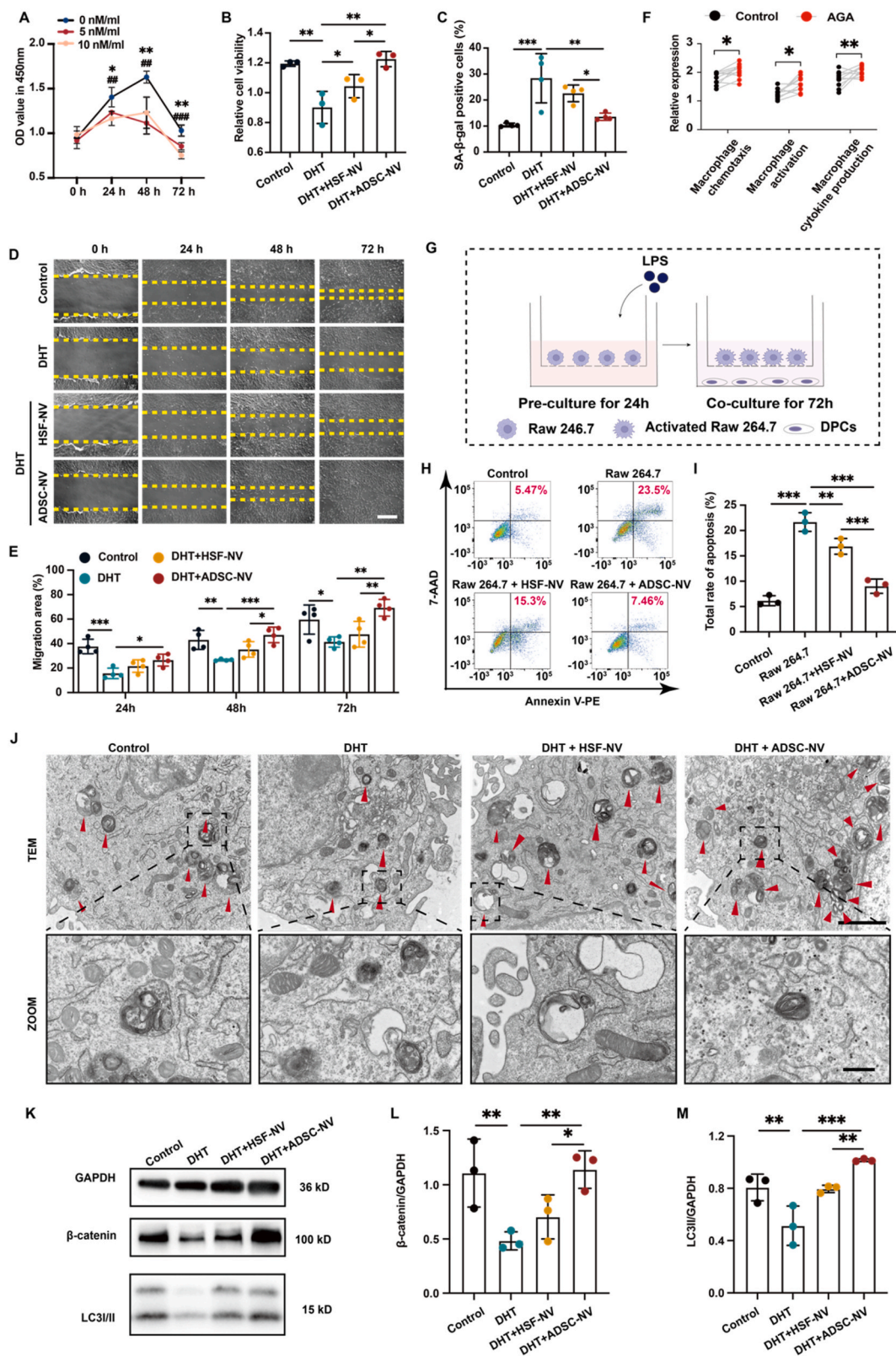


Fig. 2. Protective effect and potential mechanism of CNVs on DPCs injured by DHT and macrophages. A) Effects of various concentrations of DHT on the viability of DPCs, as shown by CCK-8 assays (n = 3). B) Viability of DHT-injured DPCs treated with CNVs for 48 h (n = 3). C) Statistical data on the proportion of senescent cells in each group was counted in the same random area (n = 4). D) Effect of CNVs on DHT-injured DPC migration at every indicating time; scale bar: 50 μ m. E) Relative migration of DHT-injured DPCs in each group (n = 4). F) Relative expression of macrophage chemotaxis, activation, and cytokine production abundances in the frontal alopecia region of AGA patients in GSE212301. G) Schematic diagram of the co-culture of DPCs with LPS-activated Raw 264.7 macrophages. H) Apoptosis cells of macrophage-injured DPCs treated with CNVs for 48 h were determined by an apoptosis kit. I) Statistical data on the proportion of apoptosis cells in each group (n = 3). J) Cellular ultrastructure in each group was detected by TEM, and red arrows indicated autophagosomes; scale bar: 2 μ m and 500 nm. K) Change in LC3 and β -catenin expression. L) Relative expression of β -catenin (n = 3). M) Relative expression of LC-3II (n = 3). (*p < 0.05, **p < 0.01, ***p < 0.001).

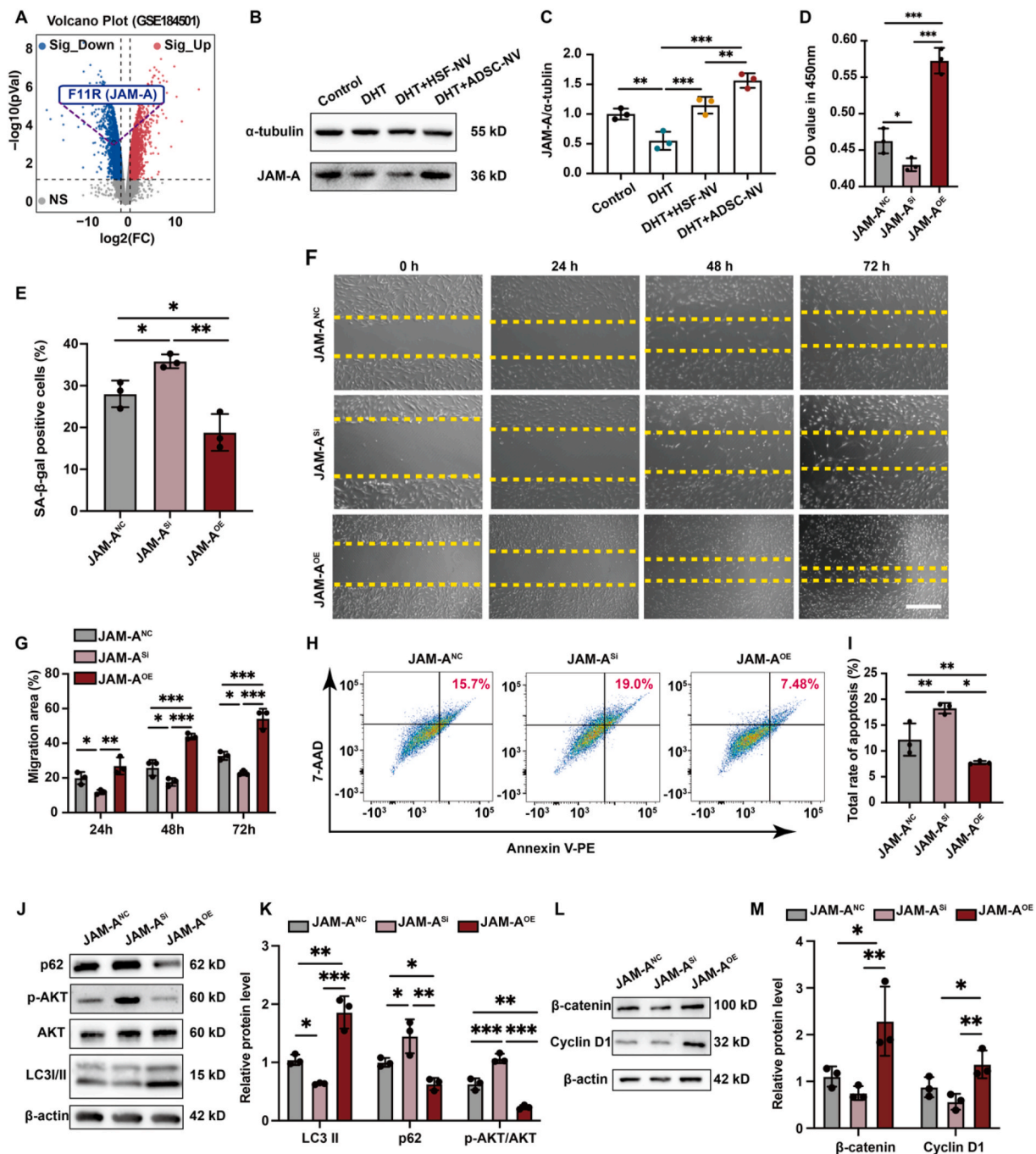


Fig. 3. JAM-A protein plays a core role in ADSC-NVs-mediated AGA hair regrowth. A) Volcano plot of the GSE184501 microarray data set, and JAM-A significantly downgraded. B) Change in JAM-A expression. C) Relative expression of JAM-A. D) Viability of DPC cell lines treated with DHT for 48 h. E) Statistical data on the proportion of senescent cells in each group was counted in the same random area. F) Effect of DHT on DPC cell line migration at every indicating time; scale bar: 50 μ m. G) Relative migration of DHT-injured DPC cell lines in each group. H) Apoptosis cells of DPC cell lines were injured with macrophages for 48 h. I) Statistical data on the proportion of apoptosis cells in each group. J) Change in LC3, AKT, AKT phosphorylation, and p62 expression. K) Relative expression of LC-3II, p62, and AKT phosphorylation. L) Change in Cyclin D1 and β -catenin expression. M) Relative expression of Cyclin D1 and β -catenin. (n = 3 per group, *p < 0.05, **p < 0.01, ***p < 0.001).

Subsequently, we quantified the levels of the AKT pathway, which regulates autophagy activity, and the indicators β -catenin and Cyclin D1, which quantify the levels of the Wnt/ β -catenin pathway, in addition to the autophagy-reflective markers LC3 and p62. Increased expression of LC3-II and decreased levels of p62 and AKT phosphorylation in the DHT-damaged culture environment of the JAM-A-overexpressing DPCs are typically indicative of enhanced autophagy activity (Fig. 3J and K). Meanwhile, the upregulation of Cyclin D1 and β -catenin signifies an

increase in the activity of the Wnt/ β -catenin pathway (Fig. 3L and M). The findings of this study indicate that the JAM-A protein is a crucial component in ADSC-NVs-mediated AGA hair regrowth.

2.5. Characterization of a JAM-A@NV-enriched thermosensitive sustained-release platform

Extrusion-prepared CNVs serve as effective drug carriers and exhibit

enhanced uptake by receptor cells, rendering them a highly promising drug delivery system [35]. As a result, cell lines of interference ADSCs and overexpression of the JAM-A protein were generated (Figs. S9A and B, Supporting Information). Additionally, JAM-A^{OE}@NV, which was extruded to transport a substantial quantity of JAM-A proteins, was obtained (Fig. S9C, Supporting Information). However, the primary limitations of exosomes and CNVs strategies are their short half-life and rapid in vivo clearance [36]. To mitigate the aforementioned limitations, it has been demonstrated that exosome-loaded hydrogels can produce sustained therapeutic effects [37,38]. The present study utilized

poloxamer 407 temperature-sensitive hydrogel, which has been shown to exhibit exceptionally low cytotoxicity and the ability to postpone nanoparticle release [39,40], to achieve sustained release of JAM-A^{OE}@NV and thereby increase its in vivo retention time.

CCK8 and live/dead staining were employed to assess the impact of poloxamer 407 hydrogel on DPCs prior to the fabrication of the JAM-A@NV Gel (Fig. 4A and B). Following the seeding of DPCs onto the hydrogels, no discernible dead cells were detected. In order to assess the thermosensitivity effectiveness of hydrogels at the macroscopic level, we initially employed the inversion method to examine the temperature

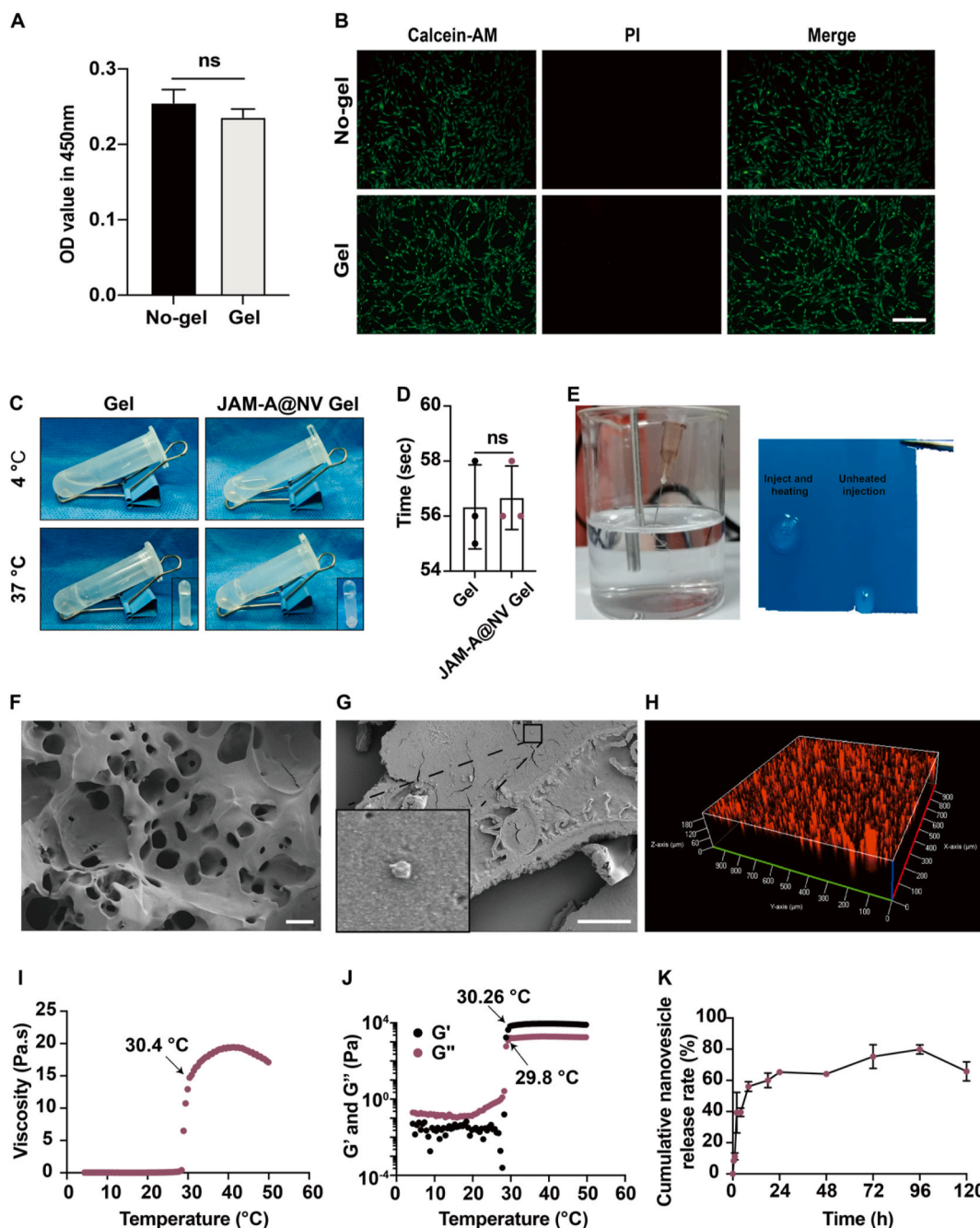


Fig. 4. Characterization of the JAM-A@NV-enriched thermosensitive hydrogel (JAM-A@NV Gel). A) The viability of DPCs cultured in a common dish or poloxamer 407 hydrogel (Gel) was evaluated by a CCK-8 assay. B) Live/dead staining of DPCs cultured on the gel or common culture dish; scale bar: 50 μ m. C) Temperature response behavior of JAM-A@NV Gel using the inversion method. D) Gelation time of JAM-A@NV Gel. E) Injectability of the JAM-A@NV Gel. F, G) Morphology of JAM-A@NV Gel; scale bars: 50 μ m and 20 μ m. H) Confocal 3D analysis of JAM-A@NV Gel. PKH26 is used to characterize JAM-A@NV (Red). I, J) Rheological properties of JAM-A@NV Gel were analyzed with temperature changes. K) The JAM-A@NV release rate behavior of JAM-A@NV Gel. (n = 3 per group, ns = not significant).

response characteristics of JAM-A@NV Gel (Fig. 4C). At 37 °C, the precursor solution of JAM-A@NV Gel gelatinized in approximately 1 min (Fig. 4D), illustrating its rapid gelatinization. The injectability of the JAM-A@NV Gel is illustrated in Fig. 4E. When the gel is warmed subsequent to injection, it significantly augments in viscosity and

diminishes in fluidity, thereby facilitating the in-situ release of the JAM-A@NV. A scanning electron microscope (SEM) analysis of the JAM-A@NV Gel revealed that it possessed a porous three-dimensional structure (Fig. 4F) and that the JAM-A@NV were encapsulated effectively (Fig. 4G). The confocal microscopy 3D view revealed that the

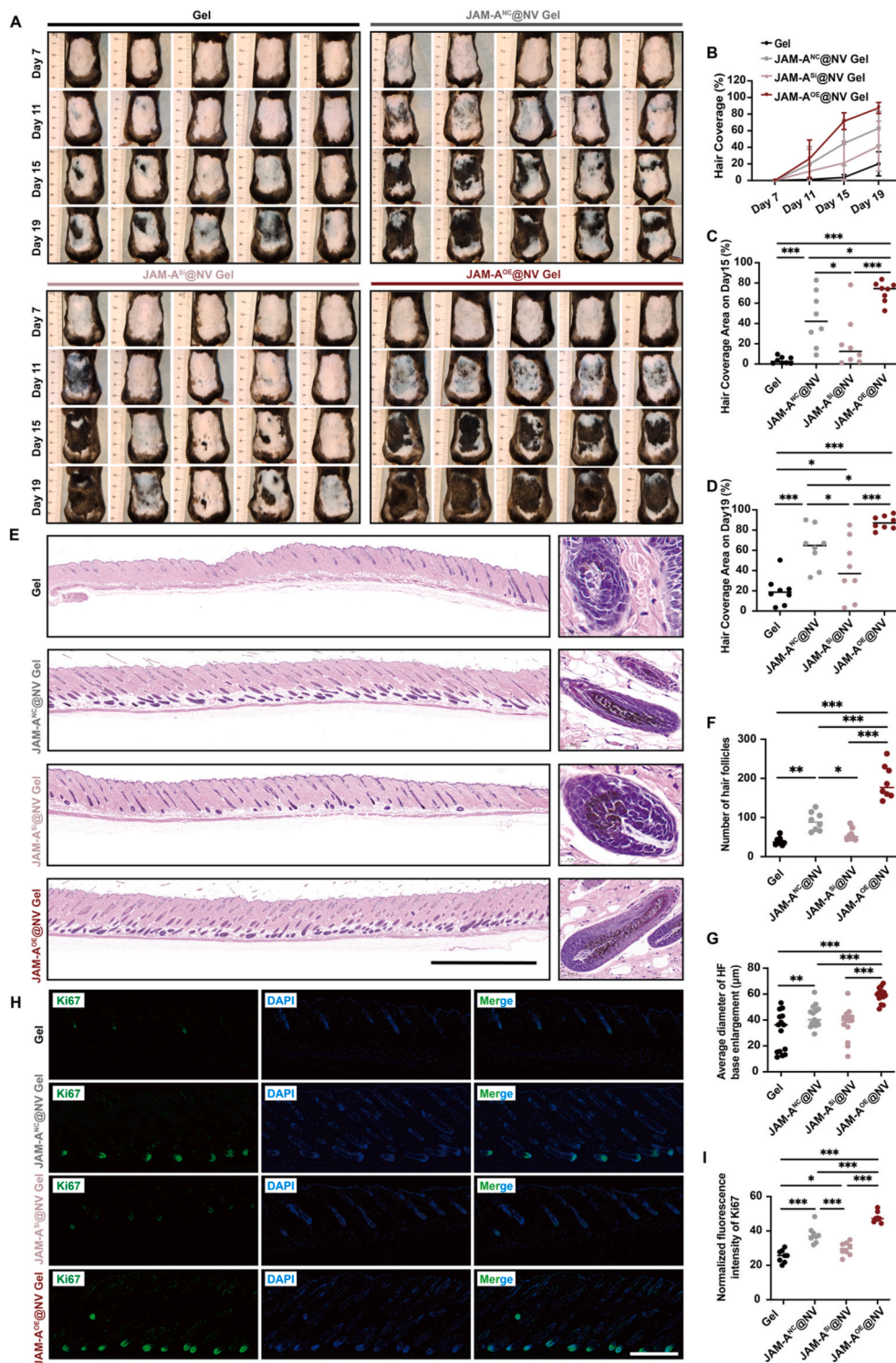


Fig. 5. Protective effect of JAM-A^{OE}@NV Gel in the AGA mouse model. A) Photographs were taken on days 7, 11, 15, and 19 after depilation (n = 8). B) The hair coverage area proportion of the dorsal skin on days 7, 11, 15, and 19 (n = 8). C, D) Statistical data of the hair coverage area proportion of the dorsal skin on days 15 and 19, respectively (n = 8). E) Representative H&E staining images of hair follicle regeneration on the dorsal skin of mice on day 21; scale bar: 2 mm. F) Statistical data on hair follicle number was counted in the same random area (n = 8). G) Statistical data on the average diameter of hair follicle base enlargement (n = 15). H) Representative Ki67 immunofluorescence staining images of hair follicle regeneration on day 21. I) Statistical data on the relative Ki67 expression of the different groups (n = 8). (*p < 0.05, **p < 0.01, ***p < 0.001).

JAM-A@NV, which was labeled with PKH-26 (red fluorescence), was uniformly dispersed throughout the hydrogels (Fig. 4H). The mechanical properties of the JAM-A@NV Gel were assessed through rheological tests. The results indicated that the gelation temperature of the gel was 30.4 °C (Fig. 4I). Furthermore, at approximately 30 °C, the storage modulus (G') of the thermo-sensitive system surpassed the loss modulus (G'') (Fig. 4J). Fig. 4K additionally illustrates the release curve of JAM-A@NV Gel. With a total release quantity of nearly 60% within the first

24 h, the JAM-A@NV reached saturation on day 4. The findings of this study suggest that the JAM-A@NV-enriched sustained-release thermo-sensitive platform was effectively developed.

2.6. Protective effect of JAM-A^{OE}@NV in vivo and in vitro

The effectiveness of JAM-A^{OE}@NV therapy was subsequently assessed using the AGA mouse model and the JAM-A downregulated

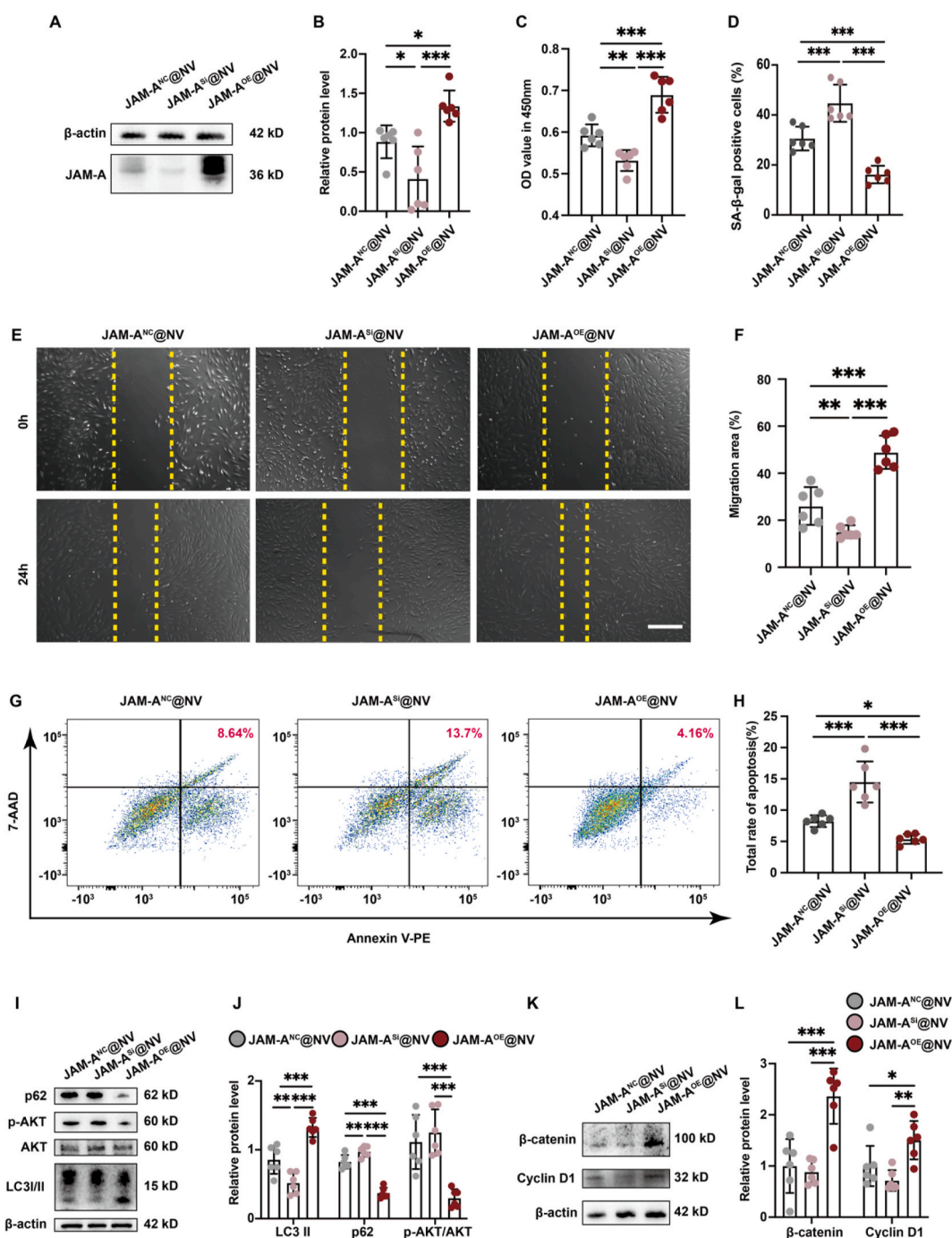


Fig. 6. Protective effect of JAM-A^{OE}@NV on JAM-A-downregulated DPC cell line injured by DHT and macrophages. A) Change in JAM-A expression. B) Relative expression of JAM-A. C) Viability of the DHT-injured, downregulated DPC cell line treatment with JAM-A@NV for 48 h. D) Statistical data on the proportion of senescent cells in each group was counted in the same random area. E) Effect of JAM-A@NV on the DHT-injured, downregulated DPC cell line migration at 24 h; scale bar: 50 μm. F) Relative migration of the DHT-injured, downregulated DPC cell line in each group. G) Apoptosis cells of the macrophages injured by downregulated DPC cell line treatment with JAM-A@NV for 48 h. H) Statistical data on the proportion of apoptosis cells in each group. I) Change in LC3, AKT, AKT phosphorylation, and p62 expression. J) Relative expression of LC-3II, p62, and AKT phosphorylation. K) Change in Cyclin D1 and β-catenin expression. L) Relative expression of Cyclin D1 and β-catenin. (n = 6 per group, *p < 0.05, **p < 0.01, ***p < 0.001).

DPCs cell line. To facilitate in vivo validation, mice were allocated into four distinct groups: the hydrogels without JAM-A@NV group (Gel group) and the hydrogels with three types of JAM-A@NV groups (JAM-A^{Si}@NV Gel group, JAM-A^{NC}@NV Gel group, JAM-A^{OE}@NV Gel group). The hair regeneration images of each group at various time points are depicted in Fig. 5A, which demonstrates a progressive decrease in the area devoid of hair. The mice assigned to the JAM-A^{OE}@NV Gel group exhibited the greatest hair coverage by day 11, indicating the most effective hair regeneration effect (Fig. 5B, Fig. S8, Supporting Information). The mice in the JAM-A^{OE}@NV Gel group exhibited significantly greater hair coverage on days 15 and 19 subsequent to hair removal (Fig. 5C and D). In contrast to the other three groups, the JAM-A^{OE}@NV Gel group was significantly higher than the other three groups. In addition, significant restorative effects were observed in the JAM-A^{NC}@NV Gel group as opposed to the JAM-A^{Si}@NV Gel group.

Ki67 immunofluorescence staining and H&E staining were utilized to histologically evaluate the effect of HF regeneration on day 21. The results of H&E staining indicated that, in comparison to the other three groups, the JAM-A^{OE}@NV Gel group demonstrated the highest efficiency in hair regrowth (Fig. 5E). The JAM-A^{OE}@NV Gel group exhibited a notably higher quantity of HF's compared to the other three groups. Furthermore, the HF's exhibited a predominantly proliferative morphology, with the most substantial expansion observed at their basal regions (Fig. 5F and G). Furthermore, the tissue slides underwent Ki67 immunofluorescence staining. The findings revealed that the JAM-A^{OE}@NV Gel group exhibited a significantly higher expression of Ki67-positive cell signals in the HF region compared to the other three groups (Fig. 5H and I). The findings of this study indicate that the application of JAM-A^{OE}@NV Gel successfully promotes the growth and maturation of HF, leading to exceptionally favorable therapeutic impacts on AGA.

To validate the findings in vitro, we initially co-incubated the three JAM-A@NV with the down-regulated DPCs cell lines. Fig. 6A and B illustrates that the JAM-A^{OE}@NV significantly restored the expression of the JAM-A protein. Subsequently, the cell lines' biological functions were restored and verified using the identical approach as the prior validation (Fig. 6C–H, Fig. S9D, Supporting Information). In comparison to the other two JAM-A@NV, the results demonstrated that the JAM-A^{OE}@NV significantly enhanced the proliferation and migration of DPCs while decreasing their senescence and apoptosis. In addition, the JAM-A^{NC}@NV exhibited substantial protective effects in comparison to the JAM-A^{Si}@NV. Finally, markers associated with the autophagy and Wnt/ β -catenin pathways were identified (Fig. 6I–L). The protein levels of LC3-II, Cyclin D1, and β -catenin increased significantly when the down-regulated DPCs cell lines were co-incubated with JAM-A^{OE}@NV. Conversely, the protein levels of p62 and AKT phosphorylation decreased significantly. These findings indicate that JAM-A^{OE}@NV plays a substantial role in facilitating the activation of the autophagy and Wnt/ β -catenin pathways, thereby rescuing the phenotype of the down-regulated DPCs cell lines.

As demonstrated by the aforementioned findings, JAM-A^{OE}@NV Gel is an effective method for promoting AGA HF regeneration and a substantial quantity of JAM-A proteins delivered via JAM-A^{OE}@NV are required to activate the autophagy and Wnt/ β -catenin pathways, thereby enhancing the biological function of damaged DPC cells.

3. Discussion

The complex pathogenesis of AGA involves multiple factors, including genetics, abnormal androgen metabolism, and inflammatory responses, resulting in a paucity of efficacious and side-effect-free biological agents being reported [41]. CNVs are potential drug delivery mediators by directly extruding cells and forming exosome-like nanovesicles that possess the high yield and biocompatibility [42]. Inspired by this, we introduced ADSC-NVs for AGA hair regeneration and explored the potential repair mechanisms. Notably, emerging studies suggests that engineering CNVs can serve as a more effective means of

disease treatment, providing clues for the efficient treatment of AGA [35].

The normal hair growth cycle undergoes a repetitive sequence of anagen, catagen, and telogen. In patients with AGA, hyperactivation of androgen receptors by DHT in DPCs will downregulate the expression of Wnt10b and β -catenin, thereby inhibiting the classical Wnt/ β -catenin signaling pathway, which is essential for the transition of HF's from the telogen to the anagen [43]. Additionally, inflammatory cell infiltration was present in AGA scalp HF's, which significantly reduces the efficacy of minoxidil [19,20]. These imply abnormal androgen metabolism and inflammation response plays a central role in the progression of AGA, consistent with the enrichment analysis in this study. ADSCs and their exosomes are well-known for the remarkable Wnt pathway activation and immunomodulation in tissue repair [44,45]. CNVs retain the original cell membrane protein structure and have a high yield, displaying remarkable similarities to exosomes in terms of physical properties, key protein markers, liposome properties, and in vitro and in vivo behaviors [42]. Based on this, we introduced ADSC-NVs for the first time into AGA therapy and their key role in the regulation of pathogenesis has been explored.

Autophagy is a vital cellular process that sustains cell homeostasis by degrading misfolded or damaged proteins and dysfunctional organelles [46]. Autophagy is an indispensable process for the self-renewal and differentiation of epidermal and dermal stem cells within the skin, as well as being crucial for hair growth [47,48]. Previous studies have reported that autophagy is upregulated during the anagen of HF's, and it has been substantiated that specific small molecule inducing autophagy promote the transition of HF's from the telogen to the anagen [49,50]. Therefore, modulation of autophagy may emerge as a significant therapeutic strategy for AGA hair regeneration therapy. JAM-A is a critical adhesion protein that participates in various physiological and pathological processes, including embryonic development, maintenance of normal tissue architecture, wound healing, and angiogenesis [51,52]. Shu et al. [53] found that a hyperglycemic environment can suppress the expression of JAM-A in mesenchymal stem cells and overexpression of JAM-A can restore the biological function of cells, reducing cell apoptosis, and upregulate the expression of cyclin D1, thereby promoting wound healing. Previous studies have demonstrated that downregulation of JAM-A expression leads to activation of the AKT pathway, which prevents the activation of the autophagy pathway in healthy cells and accelerates cellular senescence [33,34]. Therefore, this study indicates a novel mechanism by which JAM-A proteins delivered by ADSC-NVs affects hair regeneration through the autophagy pathway. Regarding whether JAM-A engineered delivery therapy has a more positive effect on AGA hair regrowth, we conducted further research.

Subsequently, a bioinspired engineered platform utilizing ADSC nanovesicles embedded in a thermosensitive hydrogel was developed in this study. This platform was further enhanced by the incorporation of JAM-A^{OE}@NV. The objective of this design was to effectively stimulate hair follicle regrowth in AGA, as demonstrated in Fig. 7. The utilization of mechanical extrusion in the production of JAM-A^{OE}@NV effectively addressed the existing issues of low yield and high cost associated with exosomes. Meanwhile, the implementation of thermosensitive hydrogels addressed the limitations associated with their short half-life and rapid in vivo clearance. In addition, our study confirmed that the JAM-A^{OE}@NV treatment leads to a significant activation of the autophagy and Wnt/ β -catenin pathways in DPCs in response to both DHT and macrophage-induced damage. Furthermore, the application of JAM-A^{OE}@NV Gel significantly improved the efficiency of hair regeneration in mice with AGA. Hence, the utilization of the engineered ADSC nanovesicle hydrogel used in this study demonstrates its capacity to effectively deliver a substantial quantity of reparative proteins, thereby facilitating the process of hair regeneration in individuals affected by AGA.

In summary, this study has certain limitations, but it also provides a theoretical basis for the follow-up research. HF's are complex micro-

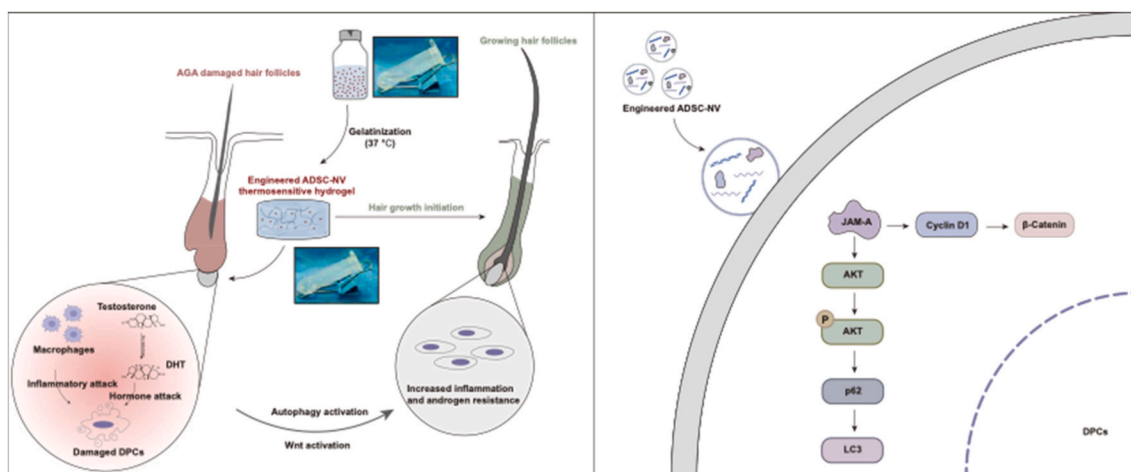


Fig. 7. Overview diagram of the mechanism of JAM-A^{OE}@NV Gel promoting AGA hair regeneration.

organs where the intricate interplay of vascularization, communication between skin epidermal-derived cells and DPCs is a hot topic in the current research field. The potential for engineered ADSC-NVs to modulate the intrinsic communication patterns represents an area ripe for further investigation. Meanwhile, next studies need to further explore autophagy mechanisms. The autophagy pathway can be further divided into macroautophagy, microautophagy, and molecular chaperone mediated autophagy [54]. Based on the organelles targeted for degradation, it can be further divided into endoplasmic reticulum autophagy and mitochondrial autophagy. Hence, the specific autophagic mechanisms in DPCs mediated by JAM-A^{OE}@NV requires us for further exploration in the future to facilitate the development of clinically effective targets.

4. Conclusion

Overall, we propose a new theory of engineered ADSC-NVs promoting AGA hair regeneration and explore the potential mechanisms of action. DPCs in the HFs of AGA patients are damaged by DHT and inflammation, which triggered the blockage of HFs entry into the anagen. JAM-A protein transferred by ADSC-NVs promotes autophagy and Wnt/ β -catenin pathways in DPCs in response to both DHT and macrophage-induced damage. Subsequently, we pioneered the introduction of engineered ADSC-NVs with overexpressed JAM-A into thermosensitive hydrogels for efficient delivery of high-yield restorative JAM-A proteins and thus enhanced hair regeneration in cases of AGA. In summary, this study not only provides a new perspective on cell-free regeneration therapies for AGA, but also this innovative approach holds significant potential for clinical application and translation.

5. Experimental section

5.1. Bioinformatics analysis

The AGA-related datasets (GSE212301, GSE90594, and GSE184501), were acquired from the GEO (Gene Expression Omnibus) database for subsequent analysis. The Weighted Gene Co-expression Network Analysis (WGCNA) method was utilized to identify the most pertinent module genes associated with AGA. Subsequently, the GeneMANIA online database (<http://genemania.org/>) was employed to investigate the co-expression network of these genes. To gain a comprehensive understanding of the role of AGA-related genes, we utilized the DAVID database (<https://david.ncifcrf.gov/>) to conduct enrichment analysis, encompassing Gene Ontology (GO) and Kyoto Encyclopedia of Genes and Genomes (KEGG). Furthermore, we obtained the gene sets for macrophage chemotaxis, activation, and cytokine

production abundances from the MSigDB database (<https://www.gsea-msigdb.org/>). To assess the levels of macrophage chemotaxis, activation, and cytokine production abundances in AGA patients, we employed the ssGSEA algorithm. The methods for implementing bioinformatics analysis in detail were previously described [55].

5.2. Cells culture and treatment

Human DPCs were obtained from human HF tissue and cultured in Low glucose Dulbecco's Modified Eagle Medium (DMEM, Cytiva, China) at 37 °C. The medium contained 10% (v/v) fetal bovine serum (FBS, Gibco, Gaithersburg, USA) and 1% (v/v) penicillin/streptomycin (P/S, Yeasen biotechnology, China). Macrophages (Raw 264.7) were procured from Zishan Biotechnology (Servicebio, China), while human ADSCs and HSF were obtained from the department of Burn Surgery affiliated with First Affiliated Hospital of Naval Medical University. The ADSCs were cultured in specialized culture medium (Oricell™, Cyagen Biosciences, China), while the HSF and Raw 264.7 were cultured in DMEM with low and high glucose concentrations (10% FBS and 1% P/S, respectively). Primary cells (passages 3 to 6) were utilized in this study.

5.3. Preparation and isolation of nanovesicles

Cellular nanovesicles were extracted from ADSCs and HSF. The cells attained a confluency of 80%–90% and were subsequently rinsed twice with PBS. Cellular pellets were then harvested and subsequently reconstituted in PBS. The extrusion device was assembled in advance in accordance with the instructions provided by the manufacturer (Whatman, United States) and its vacuum tightness was stringently inspected. Following this, the cell suspension was compressed according to the gradient of filter membrane pore size (5 μ m, 1 μ m, 0.8 μ m, 0.4 μ m, 0.2 μ m, 0.1 μ m) using a mini-extruder (Morgtec, Shanghai, China) in order to obtain nanovesicles. The suspension of compressed nanovesicles was then filtered using a 0.22 μ m filter and subsequently ultracentrifuged at 100000g for a duration of 70 min, and repeated twice at 4 °C. This process was carried out in order to obtain a purified solution of nanovesicles. The nanovesicles were then stored at a temperature of –80 °C until further use.

5.4. TEM

The methodology employed for observing the microstructure of the nanovesicles was identical to that utilized for exosomes. To summarize, the nanovesicles were fixed using a 2% paraformaldehyde solution, washed, and carefully placed onto Formvar-carbon-coated grids. Subsequently, the nanovesicles were washed again, dried, and observed

using a transmission electron microscope (TEM, Hitachi H7800, Japan). The cells were subjected to fixation by immersing the cell pellets in a solution containing 2.5% glutaraldehyde overnight, followed by fixation with a solution containing 1% osmium acid for a duration of 2 h. The sample was then dehydrated using a series of graded ethanol solutions, followed by embedding in epoxy resin and subsequent preparation into ultra-thin sections. Following that, the sections were treated with uranyl acetate and lead citrate stains, and subsequently examined using TEM.

5.5. Size detection and labeling of nanovesicles

The size of nanovesicles was determined using a NanoFlow flow cytometer (Apogee A50-micro, Apogee) in accordance with the guidelines provided by the manufacturer. The nanovesicles were labeled by staining them with PKH-26 (Sigma, Aldrich, USA). To summarize, PKH-26 solution was introduced to a specific quantity of nanovesicles and incubated for 10 min at room temperature, while being kept away from any sources of light. Following that, the stained nanovesicles were collected using a 100 kDa ultrafiltration tube (Millipore, CA, United States) and were co-incubated with the for a duration of 12 h. Subsequently, the cells were fixed in 4% paraformaldehyde solution for a duration of 10 min. The cytoskeleton was then labeled using phalloidin (Yeasen biotechnology, China), while the nuclei were stained with DAPI (Boster biotechnology, China), following the guidelines provided by the respective manufacturers. Subsequently, the nanovesicle-loaded cells were examined using a laser scanning confocal microscope (LSCM, SP8, Leica).

5.6. Western blot analysis

Nanovesicle proteins and cell proteins were subjected to separation using SDS-polyacrylamide gel electrophoresis. Subsequently, the proteins were transferred onto PVDF membranes (Millipore, USA). The membranes were blocked using protein-free rapid blocking buffer (Epizyme Biomedical Technology, Shanghai, China) for a duration of 30 min. Subsequently, they were incubated with CD63 (1:1000, ab134045, Abcam) or TSG101 (1:1000, ab125011, Abcam) or Calnexin (1:1000, ab133615, Abcam) or β -catenin (1:1000, ab32572, Abcam) or LC3B (1:1000, ab192890, Abcam) or GAPDH (1:4000, 60,004-1-Ig, Proteintech) or α -tubulin (1:1000, 2144S, Cell Signaling Technology) or JAM-A (1:1000, 36–1700, Invitrogen) or p62 (1:1000, ab109012, Abcam) or β -actin (1:1000, GB11001-100, Servicebio) or AKT (1:1000, 4685, Cell Signaling Technology) or phospho-Akt (1:1000, 4060S, Cell Signaling Technology) or Cyclin D1 (1:1000, 60186-1-Ig, Proteintech) primary antibodies overnight at 4 °C. The membranes were then incubated with a horseradish peroxidase-conjugated secondary antibody for a duration of 2 h at room temperature. Subsequently, a chemiluminescence imaging system (Tanon, Shanghai, China) was utilized to generate the protein bands. In addition, quantitative analysis was conducted using the ImageJ software (Bethesda, MD, USA).

5.7. Experimental animals model establishment, treatment and repair evaluation

The AGA model was developed in accordance with a previously reported study [23]. The animal operations conducted in this study were granted approval by the Scientific Investigation Committee of Shanghai Tongji University, in accordance with the guidelines set forth by the Animal Ethics Committee of the Shanghai East Hospital, which is affiliated with the Tongji University School of Medicine. To summarize, 6-week-old male C57BL/6 mice were procured and allowed to adapt to cages for one week. Subsequently, the AGA model mice received intraperitoneal injections (0.1 mL) containing 10 mg/mL solution of DHT (Solarbio biotechnology, China), dissolved in corn oil. These injections were administered one day prior to hair removal and on days 5 and 13 following hair removal. In the context of nanovesicle treatment, a

dosage of 200 μ g nanovesicles was administered via subcutaneous injection into the dorsal skin using either 100 μ L of PBS or hydrogel as the carrier. Minoxidil was applied topically daily as a positive control. The mice were then anesthetized using isoflurane gas via inhalation. Subsequently, the growth patterns of the dorsal skin were observed and recorded on days 7, 11, 15, and 19 following the depilation procedure. Finally, the mice were euthanized on the 21st day in order to collect tissue samples from the dorsal skin.

The skin tissue samples were fixed in a 4% paraformaldehyde solution for a duration of 72 h. Following the process of gradient ethanol dehydration and paraffin embedding, the samples underwent sectioning into 5 μ m sections for subsequent analyses. In this study, the sections underwent staining with hematoxylin and eosin (H&E) for the purpose of histological analysis. In addition, immunofluorescence analysis was conducted using a primary antibody solution for Ki67 (ab15580, Abcam), as described in our previous research [56]. Furthermore, the nuclei were stained using DAPI.

5.8. Cell proliferation and migration ability assay

The proliferation of DPCs was assessed utilizing the CCK-8 (Beyotime biotechnology, China) cell counting kit. DPCs were cultured in a 96-well plate in accordance with the manufacturer's instructions before being exposed to varying concentrations of nanovesicles (0, 50, 100, 200 μ g/mL) or DHT (0, 5, 10 nM/mL). To carry out the CCK-8 assay, 10 μ L of CCK-8 solution was added to each well for 2 h at 37 °C; subsequently, the absorbance was measured at 450 nm using a microplate reader (BioTek Epoch, USA).

In order to investigate the migration of cells, DPCs were seeded into six-well plates and cultured to ~80% confluency. After scraping the cell monolayer vertically in each well with a 200 L tip, the wells were washed 2–3 times with PBS. Subsequently, an optical microscope (Olympus, Tokyo, Japan) was used to capture optical images of the samples every 24 h. The scratched area was then analyzed using ImageJ software, and the cell migration rate was calculated as the ratio of the migrated scratch area to the initial scratch area.

5.9. Senescence-associated β -galactosidase activity assay

Serum-free DMEM, with or without nanovesicles, was treated with DPCs for a duration of 48 h under the experimental design. Subsequently, the mixture was rinsed 2–3 times with PBS. The washed cells were then fixed with β -Gal fixed solution (Solarbio biotechnology, China) for 15 min at room temperature. After incubating fixed cells for 16 h at 37 °C without CO₂, they were stained with SA- β -gal staining solution (Solarbio biotechnology, China). The SA- β -gal-positive cells were examined the next day using an optical microscope.

5.10. Cell apoptosis flow cytometry detection

A cell model for inflammatory injury was established in accordance with a previously documented study [57]. Raw 264.7 cells were cultured in transwell chambers (Corning Costar, Cambridge, MA) and subsequently exposed to LPS for a duration of 24 h. Following this, the transwell chambers were relocated to the 6-well culture plates that had been previously seeded with DPCs. The culture media was then substituted with serum-free DMEM, either with or without the inclusion of nanovesicles. Following a 72-h co-culturing period, the DPCs were collected and subjected to staining and analysis as per the guidelines provided in the flow apoptosis kit instructions (Servicebio, China).

5.11. Characterization of nanovesicle-loaded hydrogel

The JAM-A@NV Gel was prepared by thoroughly stirring and mixing Poloxamer 407 hydrogel (Solarbio biotechnology, China) and PBS containing JAM-A@NVs (v/v, 20%), within an ice bath. In addition, a

Calcein/PI cell viability/cytotoxicity assay kit (Beyotime biotechnology, China) was utilized to assess the potential toxicity of Poloxamer 407 hydrogel towards DPCs.

To facilitate the examination of the microstructure of the JAM-A@NV Gel, the hydrogel underwent a pre-freeze drying using a vacuum freeze dryer (SCIENTZ-10 N, SCIENTZ, China) for a duration of 36 h. Subsequently, the sample was acquired to examine its microstructure using a scanning electron microscope (SEM, ZEISS GeminiSEM 300, ZEISS, Germany). In addition, a Haake Mars60 rotational rheometer (Thermo Scientific, USA) was used to conduct the viscosity and rheological characterization studies. The experimental parameters include a temperature range spanning from 4 °C to 49 °C, with a temperature increment of 3 °C. The viscosity modulus was measured at a shear rate of 10 S⁻¹, while the rheological modulus was determined at a frequency of 1 Hz. Additionally, the amplitude used for the measurements was set at 1%.

5.12. Release profile of nanovesicles from hydrogel

A bicinchoninic acid protein assay kit (Epizyme Biomedical Technology, Shanghai, China) was employed to analyze the release profile of nanovesicles from the hydrogel. In this experimental procedure, a volume of 200 µL of hydrogel solution, which contained 50 µg of nanovesicles, was introduced into the modified transwell chambers of a 24-well plate. The plate was promptly placed in an incubator set at a temperature of 37 °C for a duration of 2 min, allowing the hydrogel to completely solidify. Next, 500 µL of PBS was added to the 24-well plate, ensuring complete contact with the transwell chambers. The plate was subsequently returned to a temperature of 37 °C. As per the time points previously documented [58], the BCA protein assay was conducted by extracting 20 µL of PBS from the plates, and subsequently, the release curves of nanovesicles were graphed.

5.13. Statistical analysis

The numerical data were represented as the mean ± standard deviation. The statistical analysis involved conducting multiple group comparisons using one-way ANOVA, and performing two group comparisons using Student's sample *t*-test with SPSS 26.0 software (IBM, NY, USA). The results were then visualized using GraphPad Prism software (version 9.0, La Jolla, CA). *P* values < 0.05 were considered statistically significant.

Ethics approval and consent to participate

All the animal care and experimental protocols were performed in agreement with the rules of the Scientific Investigation Committee of Shanghai Tongji University affiliated to Tongji University School of Medicine.

CRediT authorship contribution statement

Jiachao Xiong: Writing – original draft, Visualization, Software, Formal analysis. **Zhixiao Liu:** Writing – review & editing, Visualization, Formal analysis. **Lingling Jia:** Methodology, Formal analysis. **Yulin Sun:** Validation, Methodology. **Rong Guo:** Software. **Tingting Xi:** Validation. **Zihan Li:** Validation. **Minjuan Wu:** Writing – review & editing, Validation, Funding acquisition. **Hua Jiang:** Writing – review & editing, Visualization, Validation, Funding acquisition. **Yufei Li:** Writing – review & editing, Validation, Software.

Declaration of competing interest

The authors declare no competing financial interests or personal relationships that could have influenced the work reported in this paper.

Data availability

All datasets generated for this study are included in the article/Supplementary Material, further inquiries can be directed to the corresponding authors.

Acknowledgements

This work was supported by the Featured Clinical Discipline Project of Shanghai Pudong Fund (Grant No. PWYts2021-07), the East Hospital Affiliated to Tongji University Introduced Talent Research Startup Fund (Grant No. DFRC2019008) and the National Natural Science Foundation of China (Grant No. 32071186). We thank Bullet Edits Limited for the linguistic editing and proofreading of the manuscript.

Appendix A. Supplementary data

Supplementary data to this article can be found online at <https://doi.org/10.1016/j.bioactmat.2024.02.023>.

References

- [1] G. Yang, Q. Chen, D. Wen, Z. Chen, J. Wang, G. Chen, et al., A therapeutic microneedle patch made from hair-derived keratin for promoting hair regrowth, *ACS Nano* 13 (2019) 4354–4360.
- [2] M. Manabe, R. Tsuboi, S. Itami, S.I. Osada, Y. Amoh, T. Ito, et al., Guidelines for the diagnosis and treatment of male-pattern and female-pattern hair loss, 2017 version, *J. Dermatol.* 45 (2018) 1031–1043.
- [3] F. Jimenez, M. Alam, J.E. Vogel, M. Avram, Hair transplantation: basic overview, *J. Am. Acad. Dermatol.* 85 (2021) 803–814.
- [4] A.K. Gupta, M. Venkataraman, M. Talukder, M.A. Bamimore, Finasteride for hair loss: a review, *J. Dermatol. Treat.* 33 (2022) 1938–1946.
- [5] A. Goren, T. Naccarato, Minoxidil in the treatment of androgenetic alopecia, *Dermatol. Ther.* 31 (2018) e12686.
- [6] C. Ekelem, C. Pham, N. Atanaskova Mesinkovska, A systematic review of the outcome of hair transplantation in primary scarring alopecia, *Skin Appendage Disord.* 5 (2019) 65–71.
- [7] J. Xiong, H. Hu, R. Guo, H. Wang, H. Jiang, Mesenchymal stem cell exosomes as a new strategy for the treatment of diabetes complications, *Front. Endocrinol.* 12 (2021) 646233.
- [8] S. Gurunathan, M.H. Kang, M. Jeyaraj, M. Qasim, J.H. Kim, Review of the isolation, characterization, biological function, and multifarious therapeutic approaches of exosomes, *Cells* 8 (2019).
- [9] S.C. Jang, O.Y. Kim, C.M. Yoon, D.S. Choi, T.Y. Roh, J. Park, et al., Bioinspired exosome-mimetic nanovesicles for targeted delivery of chemotherapeutics to malignant tumors, *ACS Nano* 7 (2013) 7698–7710.
- [10] J.Y. Ding, M.J. Chen, L.F. Wu, G.F. Shu, S.J. Fang, Z.Y. Li, et al., Mesenchymal stem cell-derived extracellular vesicles in skin wound healing: roles, opportunities and challenges, *Mil Med Res* 10 (2023) 36.
- [11] S.C. Tao, B.Y. Rui, Q.Y. Wang, D. Zhou, Y. Zhang, S.C. Guo, Extracellular vesicle-mimetic nanovesicles transport LncRNA-H19 as competing endogenous RNA for the treatment of diabetic wounds, *Drug Deliv.* 25 (2018) 241–255.
- [12] J. Liu, Y. Sun, X. Zeng, Y. Liu, C. Liu, Y. Zhou, et al., Engineering and characterization of an artificial drug-carrying vesicles nanoplatfor for enhanced specifically targeted therapy of glioblastoma, *Adv Mater* 35 (2023) e2303660.
- [13] L. Wang, G. Wang, W. Mao, Y. Chen, M.M. Rahman, C. Zhu, et al., Bioinspired engineering of fusogen and targeting moiety equipped nanovesicles, *Nat. Commun.* 14 (2023) 3366.
- [14] J. Zhu, Z. Liu, L. Wang, Q. Jin, Y. Zhao, A. Du, et al., Exosome mimetics-loaded hydrogel accelerates wound repair by transferring functional mitochondrial proteins, *Front. Bioeng. Biotechnol.* 10 (2022) 866505.
- [15] Y. Li, Z. Shen, X. Jiang, Y. Wang, Z. Yang, Y. Mao, et al., Mouse mesenchymal stem cell-derived exosomal miR-466f-3p reverses EMT process through inhibiting AKT/GSK3β pathway via c-MET in radiation-induced lung injury, *J. Exp. Clin. Cancer Res.* 41 (2022) 128.
- [16] P. Chen, A. Ruan, J. Zhou, L. Huang, X. Zhang, Y. Ma, et al., Extraction and identification of synovial tissue-derived exosomes by different separation techniques, *J. Orthop. Surg. Res.* 15 (2020) 97.
- [17] N.J. Hawkshaw, J.A. Hardman, M. Alam, F. Jimenez, R. Paus, Deciphering the molecular morphology of the human hair cycle: Wnt signalling during the telogen-anagen transformation, *Br. J. Dermatol.* 182 (2020) 1184–1193.
- [18] J.Y. Shin, Y.H. Choi, J. Kim, S.Y. Park, Y.J. Nam, S.Y. Lee, et al., Polygonum multiflorum extract support hair growth by elongating anagen phase and abrogating the effect of androgen in cultured human dermal papilla cells, *BMC Complement Med Ther* 20 (2020) 144.
- [19] W.R. Heymann, The inflammatory component of androgenetic alopecia, *J. Am. Acad. Dermatol.* 86 (2022) 301–302.

- [20] C.L. Chen, W.Y. Huang, E.H.C. Wang, K.Y. Tai, S.J. Lin, Functional complexity of hair follicle stem cell niche and therapeutic targeting of niche dysfunction for hair regeneration, *J. Biomed. Sci.* 27 (2020) 43.
- [21] A.K. Gupta, J. Carviel, A mechanistic model of platelet-rich plasma treatment for androgenetic alopecia, *Dermatol. Surg.* 42 (2016) 1335–1339.
- [22] Z.J. Li, H.I. Choi, D.K. Choi, K.C. Sohn, M. Im, Y.J. Seo, et al., Autologous platelet-rich plasma: a potential therapeutic tool for promoting hair growth, *Dermatol. Surg.* 38 (2012) 1040–1046.
- [23] Y.H. Jung, C.W. Chae, G.E. Choi, H.C. Shin, J.R. Lim, H.S. Chang, et al., Cyanidin 3-O-arabinoside suppresses DHT-induced dermal papilla cell senescence by modulating p38-dependent ER-mitochondria contacts, *J. Biomed. Sci.* 29 (2022) 17.
- [24] C. Jaworsky, A.M. Kligman, G.F. Murphy, Characterization of inflammatory infiltrates in male pattern alopecia: implications for pathogenesis, *Br. J. Dermatol.* 127 (1992) 239–246.
- [25] F.S. Aslani, L. Dastgheib, B.M. Banihashemi, Hair counts in scalp biopsy of males and females with androgenetic alopecia compared with normal subjects, *J. Cutan. Pathol.* 36 (2009) 734–739.
- [26] A.M. Choi, S.W. Ryter, B. Levine, Autophagy in human health and disease, *N. Engl. J. Med.* 368 (2013) 1845–1846.
- [27] J.S. Rockel, M. Kapoor, Autophagy: controlling cell fate in rheumatic diseases, *Nat. Rev. Rheumatol.* 12 (2016) 517–531.
- [28] Y. Sun, C. Chen, Y. Liu, A. Sheng, S. Wang, X. Zhang, et al., Adipose stem cells derived exosomes alleviate bronchopulmonary dysplasia and regulate autophagy in neonatal rats, *Curr. Stem Cell Res. Ther.* (2023).
- [29] C. Meng, Y. Na, C. Han, Y. Ren, M. Liu, P. Ma, et al., Exosomal miR-429 derived from adipose-derived stem cells ameliorated chondral injury in osteoarthritis via autophagy by targeting FEZ2, *Int. Immunopharm.* 120 (2023) 110315.
- [30] Y. An, F. Huang, X. Tan, S. Zhu, Y. Zhen, Y. Shang, et al., Exosomes of adipose tissue-derived stem cells promote wound healing by sponging miR-17-5p and inducing autophagy protein Ulk1, *Plast. Reconstr. Surg.* 151 (2023) 1016–1028.
- [31] X. Tang, C. Cao, Y. Liang, L. Han, B. Tu, M. Yu, et al., Adipose-derived stem cell exosomes antagonize the inhibitory effect of dihydrotestosterone on hair follicle growth by activating wnt/ β -catenin pathway, *Stem Cell. Int.* 2023 (2023) 5548112.
- [32] M. Wu, C. Xu, J. Jiang, S. Xu, J. Xiong, X. Fan, et al., JAM-A facilitates hair follicle regeneration in alopecia areata through functioning as ceRNA to protect VCAN expression in dermal papilla cells, *Precis Clin Med* 5 (2022) pbac020.
- [33] A. Lampis, J.C. Hahne, P. Gasparini, L. Cascione, S. Hedayat, G. Vlachogiannis, et al., MIR21-induced loss of junctional adhesion molecule A promotes activation of oncogenic pathways, progression and metastasis in colorectal cancer, *Cell Death Differ.* 28 (2021) 2970–2982.
- [34] H. Bao, J. Cao, M. Chen, M. Chen, W. Chen, X. Chen, et al., Biomarkers of aging, *Sci. China Life Sci.* 66 (2023) 893–1066.
- [35] X. Xu, L. Xu, C. Wen, J. Xia, Y. Zhang, Y. Liang, Programming assembly of biomimetic exosomes: an emerging theranostic nanomedicine platform, *Mater Today Bio* 22 (2023) 100760.
- [36] T. Imai, Y. Takahashi, M. Nishikawa, K. Kato, M. Morishita, T. Yamashita, et al., Macrophage-dependent clearance of systemically administered B16BL6-derived exosomes from the blood circulation in mice, *J. Extracell. Vesicles* 4 (2015) 26238.
- [37] L. Luo, J. Gong, Z. Wang, Y. Liu, J. Cao, J. Qin, et al., Injectable cartilage matrix hydrogel loaded with cartilage endplate stem cells engineered to release exosomes for non-invasive treatment of intervertebral disc degeneration, *Bioact. Mater.* 15 (2022) 29–43.
- [38] S. Liu, R. Li, K. Dou, K. Li, Q. Zhou, Q. Fu, Injectable thermo-sensitive hydrogel containing ADSC-derived exosomes for the treatment of cavernous nerve injury, *Carbohydr. Polym.* 300 (2023) 120226.
- [39] X. Chen, J. Tao, M. Zhang, Z. Lu, Y. Yu, P. Song, et al., Iota carrageenan gold-silver NPs photothermal hydrogel for tumor postsurgical anti-recurrence and wound healing, *Carbohydr. Polym.* 298 (2022) 120123.
- [40] Z. Liao, W. Ke, H. Liu, B. Tong, K. Wang, X. Feng, et al., Vasorin-containing small extracellular vesicles retard intervertebral disc degeneration utilizing an injectable thermoresponsive delivery system, *J. Nanobiotechnol.* 20 (2022) 420.
- [41] G.J. Leirós, A.I. Attorresi, M.E. Balañá, Hair follicle stem cell differentiation is inhibited through cross-talk between Wnt/ β -catenin and androgen signalling in dermal papilla cells from patients with androgenetic alopecia, *Br. J. Dermatol.* 166 (2012) 1035–1042.
- [42] W.J. Goh, S. Zou, W.Y. Ong, F. Torta, A.F. Alexandra, R.M. Schiffelers, et al., Bioinspired cell-derived nanovesicles versus exosomes as drug delivery systems: a cost-effective alternative, *Sci. Rep.* 7 (2017) 14322.
- [43] G.J. Leirós, J.M. Ceruti, M.L. Castellanos, A.G. Kusinsky, M.E. Balañá, Androgens modify Wnt agonists/antagonists expression balance in dermal papilla cells preventing hair follicle stem cell differentiation in androgenetic alopecia, *Mol. Cell. Endocrinol.* 439 (2017) 26–34.
- [44] J.G. Gao, M.S. Yu, M.M. Zhang, X.W. Gu, Y. Ren, X.X. Zhou, et al., Adipose-derived mesenchymal stem cells alleviate TNBS-induced colitis in rats by influencing intestinal epithelial cell regeneration, Wnt signaling, and T cell immunity, *World J. Gastroenterol.* 26 (2020) 3750–3766.
- [45] F. Li, Z. Xu, Z. Xie, X. Sun, C. Li, Y. Chen, et al., Adipose mesenchymal stem cells-derived exosomes alleviate osteoarthritis by transporting microRNA -376c-3p and targeting the WNT-beta-catenin signaling axis, *Apoptosis* 28 (2023) 362–378.
- [46] S. Kaushik, I. Tasset, E. Arias, O. Pampliega, E. Wong, M. Martinez-Vicente, et al., Autophagy and the hallmarks of aging, *Ageing Res. Rev.* 72 (2021) 101468.
- [47] F. Belleudi, V. Purpura, S. Caputo, M.R. Torrisi, FGF7/KGF regulates autophagy in keratinocytes: a novel dual role in the induction of both assembly and turnover of autophagosomes, *Autophagy* 10 (2014) 803–821.
- [48] S. Salemi, S. Yousefi, M.A. Constantinescu, M.F. Fey, H.U. Simon, Autophagy is required for self-renewal and differentiation of adult human stem cells, *Cell Res.* 22 (2012) 432–435.
- [49] H. Rossiter, G. Stübiger, M. Gröger, U. König, F. Gruber, S. Suksee, et al., Inactivation of autophagy leads to changes in sebaceous gland morphology and function, *Exp. Dermatol.* 27 (2018) 1142–1151.
- [50] M. Chai, M. Jiang, L. Vergnes, X. Fu, S.C. de Barros, N.B. Doan, et al., Stimulation of hair growth by small molecules that activate autophagy, *Cell Rep.* 27 (2019), 3413–21.e3.
- [51] A.C. Luissint, A. Nusrat, C.A. Parkos, JAM-related proteins in mucosal homeostasis and inflammation, *Semin. Immunopathol.* 36 (2014) 211–226.
- [52] M. Wu, X. Guo, L. Yang, Y. Wang, Y. Tang, Y. Yang, et al., Mesenchymal stem cells with modification of junctional adhesion molecule a induce hair formation, *Stem Cells Transl Med* 3 (2014) 481–488.
- [53] F. Shu, J. Lu, W. Zhang, H. Huang, J. Lin, L. Jiang, et al., JAM-A overexpression in human umbilical cord-derived mesenchymal stem cells accelerated the angiogenesis of diabetic wound by enhancing both paracrine function and survival of mesenchymal stem cells, *Stem Cell Rev Rep* 19 (2023) 1554–1575.
- [54] N. Mizushima, Autophagy: process and function, *Genes Dev.* 21 (2007) 2861–2873.
- [55] J. Xiong, G. Chen, Z. Liu, X. Wu, S. Xu, J. Xiong, et al., Construction of regulatory network for alopecia areata progression and identification of immune monitoring genes based on multiple machine-learning algorithms, *Precis Clin Med* 6 (2023) pbad009.
- [56] J. Xiong, B. Ji, L. Wang, Y. Yan, Z. Liu, S. Fang, et al., Human adipose-derived stem cells promote seawater-immersed wound healing by activating skin stem cells via the EGFR/MEK/ERK pathway, *Stem Cell. Int.* 2019 (2019) 7135974.
- [57] Z. Zhang, W. Li, D. Chang, Z. Wei, E. Wang, J. Yu, et al., A combination therapy for androgenic alopecia based on quercetin and zinc/copper dual-doped mesoporous silica nanocomposite microneedle patch, *Bioact. Mater.* 24 (2023) 81–95.
- [58] J. Zeng, P. Sun, Y. Zhao, X. Fang, Z. Wu, X. Qi, Bone mesenchymal stem cell-derived exosomes involved co-delivery and synergism effect with icariin via mussel-inspired multifunctional hydrogel for cartilage protection, *Asian J. Pharm. Sci.* 18 (2023) 100799.